Raman activity of Zn_3P_2

G. Pangilinan and R. Sooryakumar
Department of Physics, The Ohio State University, Columbus, Ohio 43210

J. Misiewicz
Institute of Physics, Technical University of Wroclaw, Wroclaw, Poland
(Received 22 January 1991)

Results of nonresonant and resonant Raman scattering from single crystals of Zn_3P_2 are reported. When the exciting radiation energy is tuned well above the 1.5-eV fundamental absorption region, zone-center optical phonons are observed that are consistent with the tetragonal crystal structure of 40 atoms per primitive cell and the D_{4h}^{15} space group. For incident radiation in resonance with a weak band-edge emission at 1.534 eV, the Raman spectra are significantly altered. As the exciting frequency is tuned through the luminescence, extensive series of phonons are observed whose Raman intensities are selectively enhanced. The unusual resonant scattering is interpreted in terms of an indirect-exciton mediated process. The implications of these results in relation to the band structure of Zn_3P_2 are discussed.

I. INTRODUCTION

In marked contrast to the III-V and II-VI compounds the class of II-V materials such as Zn_3P_2, Cd_3As_2, and Zn_3As_2, have gained very little attention. The unique bonding in these semiconducting systems leads to large and complex unit cells that are characterized by vacancies dispersed throughout a tetragonally distorted fluorite lattice.[1] The occupation of different ordered atomic sites by these vacancies leads directly to the stability of many temperature-dependent polymorphs.[2] These different structures and the stability of their alloys with a continuously tunable metallic composition results in the II-V's offering a wide range of interesting structural,[3,4] transport,[5] and optical[6] properties.

Despite these features, the complexity of the crystal structure has greatly hindered progress in understanding fundamental properties of this class of materials. For example, only one band-structure calculation is available and was made under assumptions of a pseudocubic structure with the missing atoms represented by a matched pseudopotential.[7] Subsequently, refinements that included spin-orbit and crystal-field effects were introduced.[8] Further, there is no calculation nor measurement of the phonon dispersion curves for any of the II-V materials. In the growth of these materials, the relatively small free energy differences between various metastable states often result in difficulties of stabilizing a particular phase during growth. It has been only in the last few years that epitaxial techniques have been successfully applied to the growth of Zn_3As_2 and Zn_3P_2,[4,9] a step that is bound to promote more research into this class of materials.

Zn_3P_2 has distinct prominence among II-V materials for its technological promise as a solar-energy conversion device, and several papers have addressed this issue.[6,10] Its absorption edge, photoexcited-carrier lifetime, and diffusion lengths are compatible with requirements for such applications.[11] Nevertheless, critical properties regarding the fundamental energy gap (magnitude and nature, whether direct or indirect),[7,10–14] as well as an assignment of the lattice vibrations in Zn_3P_2 (and most other polymorphs) remain uncertain. The primary goal of the present work is to investigate the phonons of bulk single crystalline Zn_3P_2 by Raman scattering in order to elucidate the zone-center optical phonon frequencies and complement existing data on the infrared active vibrations. Light-scattering experiments performed under conditions resonant with the interband absorption gap were directed at providing insight into the band structure in this vicinity. Such spectra recorded around 1.53 eV reveal an unusual series of phonons which are interpreted in terms of a phonon-assisted Raman process that is mediated by an indirect exciton.

In the next section we describe the crystal structure of Zn_3P_2 and classify the lattice vibrations in terms of the irreducible representations of its point group. Section III briefly describes the experimental conditions and the samples, while Sec. IV pertains to the results of the Raman experiments. These results are discussed in Sec. V, with our conclusions provided in Sec VI.

II. CRYSTAL STRUCTURE AND SYMMETRY OF LATTICE VIBRATIONS

The ambient crystal structure of Zn_3P_2 is D_{4h}^{15} and the primitive cell contains eight formula units or 40 atoms. In fact, the symmetry of local ordering is higher than that suggested by its crystallographic classification. The structure is illustrated in Fig. 1. Barring a slight tetragonal distortion in the D_{4h}^{15} phase, the P sublattice ($\times$'s in Fig. 1) is analogous to that in the zinc-blende InP. The Zn sublattice (O's) is similar to that of fluorine in the CaF_2 structure with 25% vacant Zn sites (wedges) ordered within the lattice. Each P is surrounded by eight tetrahedral cavities, six of which are occupied by Zn atoms while two are vacant. Every Zn atom is

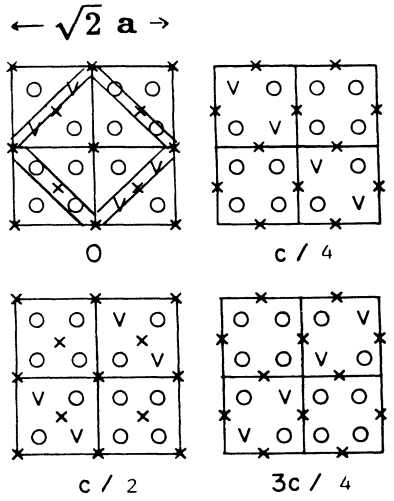

FIG. 1. The atomic positions in Zn_3P_2 with D_{4h}^{15} space group. The c axis is divided by four planes perpendicular to the c axis. The ×'s represent the P atoms on the plane, the ○'s are Zn atoms at $c/8$ above the denoted planes, and the V's are vacant Zn sites. The double lines denote the boundaries of the unit cell in the ab plane.

tetrahedrally bonded to four P atoms. The primitive cell can hence be viewed as a stacking of pseudocubic blocks, which, except for the small distortion noted above, are fluorite or zinc-blende unit cells.[3] In this model the vacancies are located only within the zinc-blende cells. It is primarily this vacancy ordering which makes the volume of the Zn_3P_2 primitive cell four times that of the fluorite subcell, and explains the lower symmetry.

The zone-center phonons of Zn_3P_2 can be expressed in terms of the irreducible representations of the D_{4h} point group as follows:

$$\Gamma_{\text{vibrational}} = 9A_{1g} + 5A_{2g} + 10B_{1g} + 4B_{2g} + 16E_g + 4A_{1u} + 10A_{2u} + 5B_{1u} + 9B_{2u} + 16E_u \ .$$

The Raman and infrared-active phonons are

$$\Gamma_{\text{Raman}} = 9A_{1g} + 10B_{1g} + 4B_{2g} + 16E_g \ ,$$

$$\Gamma_{\text{ir}} = 9A_{2u} + 15E_u \ .$$

The other modes are silent. The Raman tensors for the A_{1g} and B_{1g} modes are diagonal while those for the B_{2g} and E_g vibrations each have only two finite nondiagonal elements.

III. EXPERIMENT

The two single-crystal samples of Zn_3P_2 (A and B) utilized in this study were grown by the gas-transport method as described elsewhere.[15] Sample A was cut and polished with the tetragonal c axis [001] normal to the surface. The crystal orientation was determined by structural x-ray analysis carried out on a AFC 5 Rigaku diffractometer. The x-ray diffraction peaks were consistent with the reported D_{4h}^{15} space group. In order to identify vibrations of all symmetries it was necessary to study sample B that was oriented differently to A. Sample B was utilized in its as-grown form and the exciting beam was incident on a surface in which the c axis was lying parallel to the plane.

The Raman measurements were carried out at 10 K in backscattering with about 100-mW power. The 5308- and 6471-Å laser lines were separately utilized for the nonresonant Raman measurements. A dye (LD 700 perchlorate) laser provided the tunable radiation for the resonant studies. Photoluminescence measurements were carried out at low temperature in order to identify any radiative transitions that occur in the vicinity of the strong absorption structure observed in Zn_3P_2. Far-infrared reflectivity measurements were completed with a BOMEM interferometer at room temperature and at 40 K from sample B. A germanium bolometer or pyroelectric detector was chosen in appropriate energy ranges.

IV. RESULTS

Polarized Raman spectra measured from samples A and B for the 5308-Å exciting radiation is shown in Fig. 2. No first-order Raman active phonons were observed beyond about 380 cm^{-1}. The spectra in Figs. 2(a)–2(d) were recorded from crystal A under scattering geometries chosen to reveal specific phonon symmetries. The standard notation has been utilized where $z(x,y)\bar{z}$ denotes the incoming radiation along z being polarized along x with the backscattered ($\bar{z}$) light polarized along y. The orientation of the axes are identified at the top of Fig. 2. Several well-defined phonon modes are observed, which broadly fall into two frequency ranges; those lying below about 220 cm^{-1} and another group of vibrations between 270 and 360 cm^{-1}. This grouping is consistent, after simple scaling of the anion masses, with the Raman active vibrations from epitaxial films of Zn_3As_2 that was shown to stabilize in the D_{4h}^{15} space group.[3]

The allowed symmetries are identified in each spectra (a)–(d) of Fig. 2 and are adequate to identify A_{1g},, B_{1g}, and B_{2g} modes. These peaks are respectively identified as such by arrows in Figs. 2(b)–2(d). In order to isolate the E_g vibrations, unpolarized spectra from sample B were measured and the spectrum is shown in Fig. 2(e). The arrows on this spectrum indicate the E_g phonons. The assignment of phonon symmetries in the vicinity of laser plasma lines (L) was reconfirmed by also utilizing the neighboring 5145-Å laser radiation.

Figure 3 shows data recorded similarly to that in Fig. 2 but excited with 6471-Å radiation. A comparison between the two figures shows that, while the spectra are generally similar, the relative intensities of some of the peaks (*'s in Figs. 2 and 3) are different. For example, the 150-cm^{-1} (B_{1g}) and 210-cm^{-1} (A_{1g}) modes in Fig. 2 are absent in Fig. 3, while the 224-cm^{-1} A_{1g} peak/shoulder recorded at 5308 Å (Fig. 2) is strongly enhanced at 6471 Å (Fig. 3).

Optical measurements have confirmed that at low tem-

peratures a strong absorption exists around 1.5 eV in Zn_3P_2.[10,11] We were hence motivated to investigate the phonon spectra under resonance scattering to identify additional Raman features that may not have been revealed under the nonresonant conditions outlined above. As shown in the inset to Fig. 4 photoluminescence measurements from sample A located a weak emission band approximately 30 meV wide and centered around 1.53 eV. No emission (nor any resonant Raman features as discussed below for sample A) was detected from sample B. The luminescence structure from sample A was observed only when the exciting energy was within 160 meV from 1.53 eV. For example, the emission was quenched when excited at 1.9 and 2.2 eV.

Figure 4 shows a series of Raman spectra from sample A for different excitation energies in the immediate vicinity of the luminescence band. The energies of the exciting laser utilized in recording each of these spectra in relation to the emission band is identified by arrows in the inset to Fig. 4. The remarkable changes between spectra (a)–(d) in Fig. 4 arise when the laser photon energy is varied by only about 50 meV and these spectra bear little resemblance to those in Figs. 2 and 3. Further, the intensity of the resonant Raman peaks were as much as 3 orders of magnitude higher than those recorded under nonresonant conditions. It is also evident that several peaks in Fig. 4 are selectively enhanced when they fall on the maximum of the underlying luminescence. None of the sharp peaks in Fig. 4 were fluorescence for their absolute energies were not the same in all spectra.

In Fig. 5 we have plotted, for comparison a Raman spectrum from sample A revealing $A_{1g}+B_{1g}$ phonons that was excited with 5308-Å radiation and a spectrum measured at 8010 Å in resonance with the 1.53-eV emis-

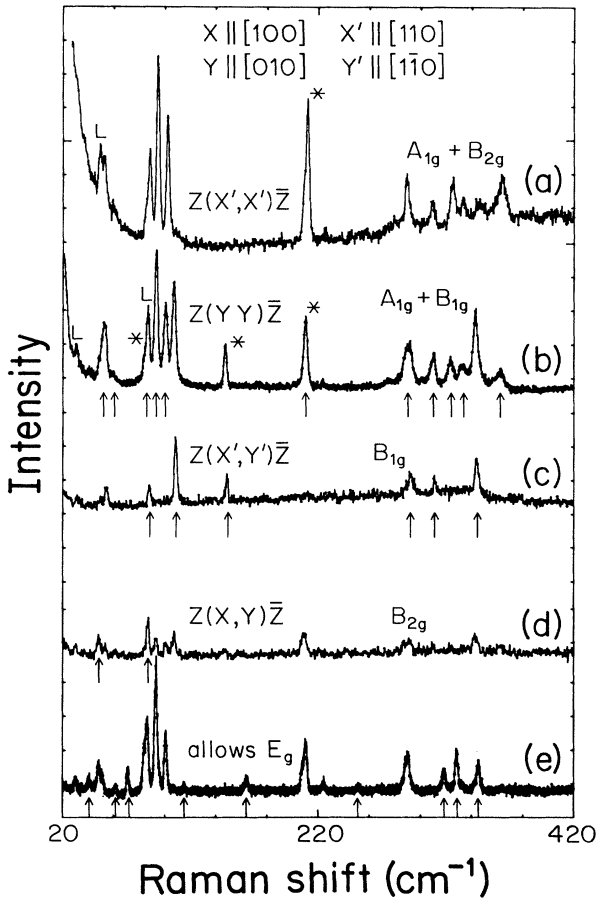

FIG. 2. (a)–(d) polarized Raman spectra at 10 K from sample A excited with 5308-Å radiation. The arrows under spectra (b), (c), and (d), respectively, identify A_{1g}, B_{1g}, and B_{2g} excitations. (e) is an unpolarized spectrum from sample B that enables the E_g vibrations to be identified (arrows). L's refer to laser plasma emissions and *'s identify peaks that are probably associated with impurities (see text).

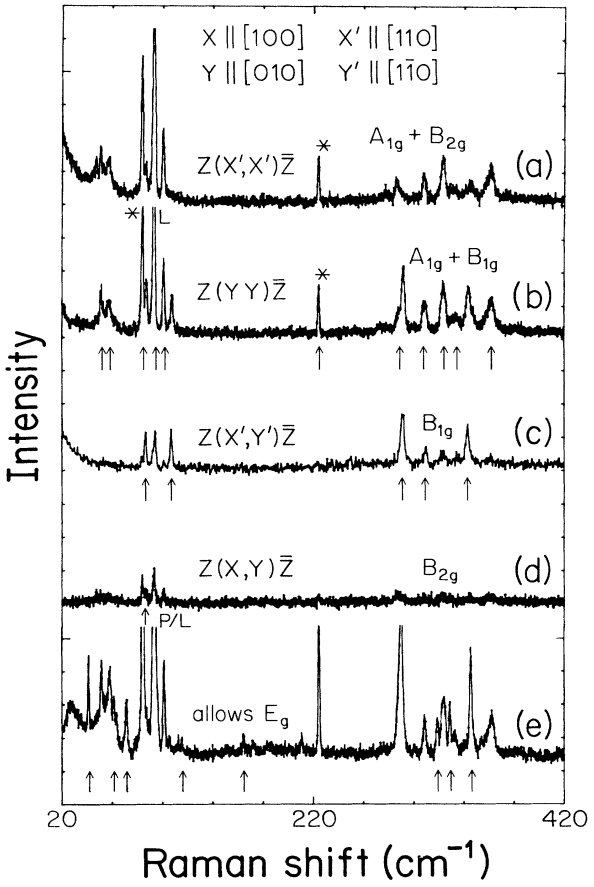

FIG. 3. (a)–(d) polarized Raman spectra at 10 K from sample A excited with 6471-Å radiation. The arrows under spectra (b), (c), and (d), respectively, identify A_{1g}, B_{1g}, and B_{2g} excitations. (e) is an unpolarized spectrum from sample B that enables the E_g vibrations to be identified (arrows). L's refer to laser plasma emission while P/L identifies a phonon lying in the vicinity of the plasma line. *'s identify peaks that are probably associated with impurities (see text).

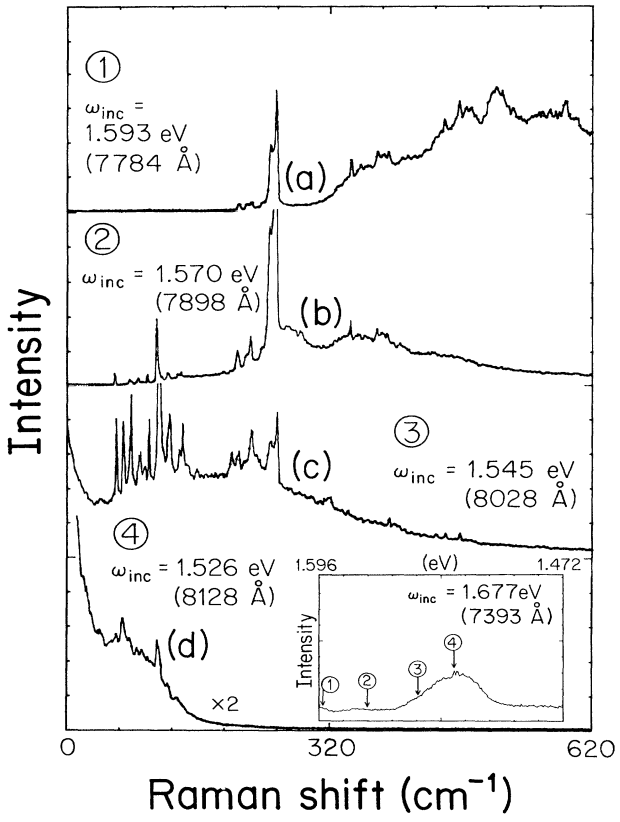

FIG. 4. Unpolarized Raman spectra from sample A measured at 10 K with the exciting frequency in resonance with the emission band shown in the inset. (a)–(d) were recorded with the relative (to the emission band) energy of incident laser radiation being indicated in the inset.

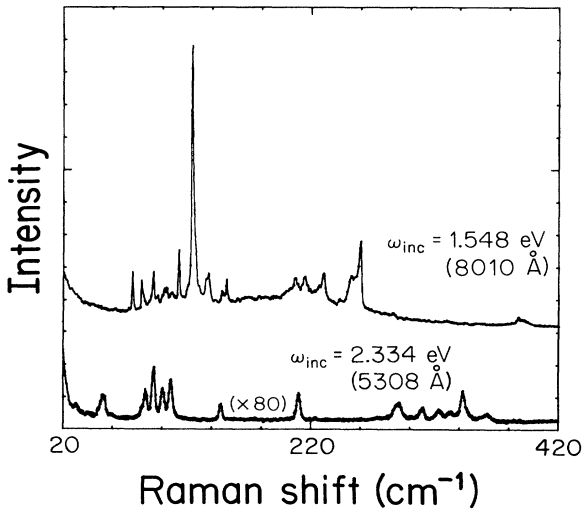

FIG. 5. A comparison between the resonant Raman spectrum measured with 8010 Å and nonresonant scattering recorded at 5308 Å. The latter allows excitations of A_{1g} and B_{1g} symmetries. Both spectra are from sample A.

sion. The peak positions in each of the spectra of Fig. 5 do not coincide, and hence they correspond to different excitations in the two situations.

V. DISCUSSION

A. Nonresonant scattering

We first discuss the nonresonant spectra of Figs. 2 and 3. Based on the analysis of Sec. II, 9 A_{1g}, 10 B_{1g}, 4 B_{2g}, and 16 E_g zone-center Raman-active phonons are supported by the D_{4h}^{15} Zn_3P_2 structure. The measured spectra show strict selection rules being satisfied in agreement with the space group. Figure 2 reveals 11 A_{1g}, 6 B_{1g}, 2 B_{2g}, and 9 E_g peaks, while in Fig. 3, recorded at 6471 Å, 11 A_{1g}, 5 B_{1g}, 1 B_{2g}, and 8 E_g peaks are identified. Other than the three extra peaks of A_{1g} symmetry and the B_{1g} mode (*'s in Figs. 2 and 3) that are discussed below, we identify the remaining peaks as Raman-active lattice vibrations in Zn_3P_2. The scattering cross section of the unobserved phonons are probably too weak to measure.

There are two peaks of A_{1g} symmetry in each of Figs. 2 and 3 that are in excess of the phonon modes predicted by group theory. It is noted that two A_{1g} peaks are observed to behave differently from all others in each of the figures. They correspond to modes at 85 and 210 cm^{-1} in Fig. 2 and 85 and 224 cm^{-1} in Fig. 3. The intensity of these particular excitations are strongly dependent on the exciting frequency and are selectively modified compared to the other peaks. This behavior suggests that these anomalous peaks are excitations that are different from the 9 A_{1g} Zn_3P_2 phonons expected of this symmetry.

These unusual additional A_{1g} modes may be derived from the acceptor states in Zn_3p_2 that is a known p-type semiconductor with the defect vacancy structure discussed in Sec. I. For example, electronic transitions within the acceptor states are possible with energies that are comparable to those of optical phonons. In GaP for instance, transition between Zn or Mg impurity levels are observed with frequencies and widths that are comparable to intrinsic phonons.[17] In addition, gap modes, which are lattice vibrations modified by impurities in the form of substitutions or interstitials, also vibrate with frequencies comparable to the pure material[18] and could account for the additional Raman peaks. The selective resonance in Figs. 2 and 3 of only these four (at 85, 150, 210, and 224 cm^{-1}) modes of the multitude of Raman peaks support their nonintrinsic origin. Intrinsic phonons should, in the absence of specific interference effects, all have the same general response to changes in the exciting radiation. Such an interference phenomenon has been observed for example, in one of the A_{1g} phonons of the chalcopyrite $AgGaAs_2$.[19] Thus, while this observed Raman activity of Zn_3P_2 is consistent with the D_{4h}^{15} space group, a definitive assignment of the three unusual A_{1g} peaks and one B_{1g} mode to acceptor states remains to be confirmed.

B. Resonant scattering

We now turn to Fig. 4 and discuss the resonant Raman spectra. First-order Raman scattering can be treated in

third-order perturbation theory. The resulting expression for the Raman efficiency thus contains two energy denominators that relate the incident and scattered photon energies to electronic levels in the solid. These levels constitute the intermediate state for the inelastic scattering event. For energies of either (incident/scattered) photon that are matched to electronic transitions, the denominators vanish and result in strong enhancements of the resonant scattering cross section. Resonant Raman scattering is therefore also an effective probe of the intermediate state and its interaction with lattice vibrations.

There are few examples in which resonant Raman scattering has been studied in indirect gap materials, with the radiation in the vicinity of the gap. Among these studies are Si and GaP, where the resonance is with a continuum rather than discrete exciton states and hence only minor resonant enhancements are seen in the one-phonon intensity.[20] On the other hand, at the indirect gap of AgBr strong resonances have allowed specific energy bands within the Brillouin zone to be probed through coupling with a series of finite wave vector ($q \neq 0$) phonons.[21] The Raman process in AgBr that involves an electric-dipole-allowed *indirect* transition may be contrasted to the electric-dipole-forbidden *direct* transitions that enabled all odd parity phonons to be observed in Cu_2O.[22] As seen below, resonant Raman scattering in Zn_3P_2 appears to be very similar to that in AgBr.

The currently available energy-level structure in Zn_3P_2 is largely based on optical data in the vicinity of the band-edge absorption.[10,11] Unfortunately, these experiments do not allow a definitive statement as to whether the gap is direct or indirect;[10] while the only available calculation of Lin-Chung[7] for a simplified crystal structure and subsequent refinements[8] favor a direct gap. Numerical values for the gap also appear to be uncertain, although evidence for a direct interband transition around 1.5 eV (at 300 K) seems to be a cautious consensus among several measurements.[10,11,13,14] This transition will move to higher energies at low temperatures, and has been identified in one study[13] to be at 1.68 eV for the temperature (10 K) utilized in the present measurements. The strong room-temperature absorption at 1.5 eV has made it difficult to unambiguously identify weak absorption transitions spanning 1.3 and 1.5 eV that have also been reported in some instances.[11,14] This unresolved status of the band structure of Zn_3P_2 compel us to provide only a tentative model to describe the resonant Raman data.

The spectra of Fig. 4 are consistent with the existence of an indirect level at about 1.53 eV at 10 K in our Zn_3P_2 samples. This is schematically illustrated in Fig. 6, which also shows the resonant scattering process. The incident photon of energy E_L, which is in near resonance with the indirect state, creates a direct (virtual) exciton via the exciton-photon interaction. Through mediation of a momentum-conserving (finite q) optical phonon it is scattered into the indirect-exciton state (energy E_1). Reemission of an optical phonon ($q \neq 0$), creates the scattered direct exciton that finally recombines emitting a photon of energy E_s. *One* of these exciton scattering steps could

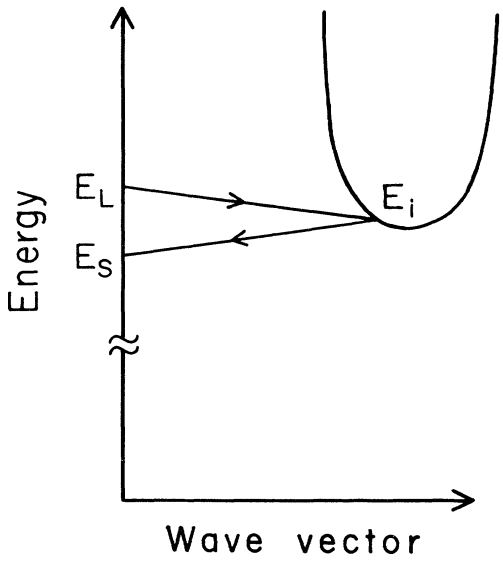

FIG. 6. Schematic of indirect level dispersion near 1.5 eV and relevant Raman scattering process involving two finite wave-vector phonons. One of the phonon-mediated scattering events shown could be replaced by an impurity-assisted event to scatter the exciton either to or from the indirect level (see text).

also occur through impurities as reported in resonant Raman scattering from bulk GaAs.[23] In this case momentum conservation is relaxed through the impurity ion, and thus only a *single* phonon is required to mediate the exciton scattering to the indirect level and back. The existence of strong electron-lattice coupling (that is compatible with the known solar-energy conversion properties of Zn_3P_2) is consistent with both these types of inelastic scattering processes.

Most of the Raman peaks evident in Fig. 4 are probably associated with phonons. While all of the large number of peaks observed in the resonant spectra are unlikely to originate from localized impurity excitations, a multitude of phonons are to be expected from lattice vibrations of the 40-atom primitive cell of Zn_3P_2. Some of the peaks in Fig. 4 are overtone excitations (for example, those at 125, 250, and 375 cm^{-1}). The one-phonon peaks seen at resonance are also not zone-center odd parity modes that may arise from a breakdown of selection rules. Infrared-active phonons at these energies were not revealed in our low-temperature reflectivity spectra (from sample B) that were very similar to those reported in Ref. 16. Further, energies of the finite q phonons involved in the resonant scattering will generally be dissimilar from those of vibrations ($q \approx 0$) recorded under nonresonant conditions. This deviation in energy thus accounts for the frequency differences in the two spectra of Fig. 5.

The linewidths of the peaks clustered between 80 and 150 cm^{-1} and 210 and 260 cm^{-1} of Fig. 4 are narrow and comparable to the one-phonon peaks of Figs. 2 and 3. While it is usual that nonresonant two-phonon scattering

processes normally give rise to relatively broad Raman peaks (since they reflect the one-photon density of states), the sharpness of the resonant phonons in Zn_3P_2 is due to the selection of only specific phonon wave vectors (Fig. 6) that will move the exciton to and from the indirect level. Such selective phonon wave-vector scattering would also hold if, as discussed above, impurities were intermediary to the scattering. The inelastic scattering spectra in this case reveals only a one-phonon scattering event and thus would account for the limited line broadening. In the absence of such impurity-mediated effects, phonons ($q \neq 0$) with little or no dispersion must dominate the scattering events depicted in Fig. 6 to yield the sharp peaks of Fig. 4.

These narrow phonon linewidths in Zn_3P_2 (Fig. IV) are reminiscent of those observed in resonant Raman scattering at the indirect gap of AgBr.[21] In this latter study, various exciton relaxation processes were revealed and their analysis yielded carrier effective masses and lifetimes. However, the lack of a definitive energy band structure for Zn_3P_2 and unavailability of its phonon dispersion branches prevent us from utilizing the spectra of Fig. 4 to similarly deduce quantitative parameters associated with the charge carriers.

The weakness and breadth of the emission band observed at 1.53 eV arises from the existence of nonradiative processes due to the indirect nature of the resonant level and reabsorption effects. The luminescence as well as the unusual series of resonant Raman peaks, while evident from sample A, were not observed from sample B, in which the c axis was oriented parallel to the surface. The absence of the radiative transitions and pronounced phonon resonances in this sample could arise from two different sources. First, due to the different crystal orientation, the optical transition connecting the ground state to the excited state may be forbidden or weakly allowed. While evidence for some dichroism exists,[11] in our opinion, this difference in the polarization dependence alone would be inadequate to explain the absence of the resonant Raman features in sample B. The other possibility could be that there is an enhancement of nonradiative processes in sample B due to a different concentration of certain impurities or defects. The possibility of exciton trapping at such specific centers could inhibit their inelastic scattering to finite wave-vector states. Such effects on the indirect-exciton lifetime may be sufficient to smear the resonance manifested in sample A.

VI. CONCLUSIONS

In summary, we have reported on the low-temperature Raman activity of single crystalline Zn_3P_2. The measurements under nonresonant conditions have revealed many of the zone-center optical phonons that are consistent with the D_{4h}^{15} crystal structure. In addition to the intrinsic phonons, three excitations of A_{1g} symmetry and one B_{1g} mode that appear to be related to acceptor states known to be present in these materials were observed.

Resonant Raman scattering measurements have revealed an unusual series of phonon excitations in the sample where the c axis is oriented normal to the incident electric field. We have interpreted these results in terms of an indirect-exciton-mediated scattering process. Comparison between the sharp peaks of the resonant and nonresonant Raman spectra reveal that the exciton relaxation process in the former is mediated either by dispersionless finite q phonons involved in a two-phonon scattering event or by an impurity aided one-phonon process. Our results suggest the existence of an indirect level lying in the vicinity of 1.53 eV at 10 K and the unusual phonon resonances to be a manifestation of strong exciton-lattice interactions in Zn_3P_2. The general resonant Raman activity of Zn_3P_2 is hence found to closely follow that in AgBr where unusual phonon-assisted transitions to indirect intermediate states were observed.

ACKNOWLEDGMENTS

Work at The Ohio State University was supported by the National Science Foundation under Contracts No. DMR 87-03980 and No. DMR 90-01647. J.M. is indebted to the Institute of Physics, Polish Academy of Sciences, for financial support under CPBP 01.04.I.2.7.

[1] *Proceedings of the First International Symposium on the Physics and Chemistry of II-V Compounds,* edited by M. J. Gelten and L. Zdanowicz (Eindhoven University of Technology, Netherlands, 1980).

[2] A. D. Izotov, A. Sanygin, and V. F. Ponomarev, and Kristallografiya **23**, 764 (1978) [Sov. Phys. Crystallogr. **23**, 429 (1978)].

[3] G. Pangilinan *et al.,* Phys. Rev. Lett. **62**, 551 (1989).

[4] D. M. Hwang *et al.,* Appl. Phys. Lett. **54**, 1160 (1989).

[5] L. G. Caron, M. J. Aubin, and J. P. Jay-Gerin, Solid State Commun. **23**, 493 (1977).

[6] M. Bhushan, Appl. Phys. Lett. **40**, 51 (1982).

[7] P. J. Lin-Chung, Phys. Status Solidi B **47**, 33 (1971).

[8] B. Dowgiallo-Plenkiewicz and P. Plenkiewicz, Phys. Status Solidi B **87**, 309 (1978).

[9] B. Chelluri *et al.,* Appl. Phys. Lett. **49**, 1665 (1986); J. Cryst. Growth **81**, 530 (1987).

[10] E. A. Fagan, J. Appl. Phys. **50**, 6505 (1979).

[11] V. Munoz, D. Decroix, A. Chevy, and J. Besson, J. Appl. Phys. **60**, 3282 (1986).

[12] V. V. Sobolev and N. N. Syrbu, Phys. Status Solidi B **64**, 423 (1974).

[13] J. M. Pawlikowski, J. Appl. Phys. **53**, 3639 (1982); Phys. Rev. B **26**, 4711 (1982).

[14] J. M. Pawlikowski, J. Misiewicz, and N. Mirowska, J. Phys. Chem. Solids **40**, 1027 (1979).

[15] J. Misiewicz *et al.,* Acta Phys. Pol. A **69**, 1127 (1986), and references therein.

[16] J. Misiewicz, J. M. Wrobel, and B. Clayman, Solid State Commun. **66**, 747 (1988).

[17]C. H. Henry, J. J. Hopfield, and L. C. Luther, Phys. Rev. Lett. **17**, 1178 (1966).
[18]A. S. Barker, A. J. Sievers, Rev. Mod. Phys. **47**, S1 (1975).
[19]J. P. van der Ziel *et al.*, Phys. Rev. B **9**, 4286 (1989).
[20]P. B. Klein, H. Masui, J. Song, R. Chang, and K. Chang, Solid State Commun. **14**, 1163 (1974).
[21]J. Windscheif and W. von der Osten, J. Phys. C **13**, 6299 (1988).
[22]P. Y. Yu and Y. R. Shen, Phys. Rev. B **12**, 1377 (1975).
[23]A. Alexandrou, C. Trallero-Giner, G. Kannellis, and M. Cardona, Phys. Rev. B **40**, 1013 (1989).